

# Bone Remodeling Process and Covid-19: A Modelling Approach

CHONTITA RATTANAKUL  
Department of Mathematics,  
Faculty of Science,  
Mahidol University,  
Bangkok,  
THAILAND

*also with*  
Centre of Excellence in Mathematics,  
MHESI,  
Bangkok,  
THAILAND

*Abstract:* - Apart from the effects on the lungs, COVID-19 caused by the severe acute respiratory syndrome coronavirus 2 (SARS-CoV-2) also has effects on bone metabolism including the bone remodelling process. The bone remodelling process involves bone formation by bone-forming cells (osteoblasts) and bone resorption by bone-resorbing cells (osteoclasts). The infection with SARS-Cov-2 decreases the inhibiting effects of Angiotensin-converting enzyme 2 (ACE2) on osteoclastic reproduction and inhibits the osteogenic ability of osteoblasts which might lead to the imbalance in the bone remodeling process. In this study, we modify the system of differential equations to investigate the effects of Covid-19 on bone formation and bone resorption. The geometric singular perturbation method is utilized to analyze the modified model theoretically. To illustrate the theoretical results, numerical investigations are also demonstrated. The results indicate that the oscillations in the numbers of osteoclastic cells and osteoblastic cells observed in the clinical evidence could still be expected when the effects of SARS-Cov-2 are incorporated, however, the oscillations occur at the higher level of the number of osteoclasts and hence more bone loss might occur when infected with Covid-19.

*Key-Words:* - Covid-19, osteoclast, osteoblast, mathematical model, geometric singular perturbation

Received: December 17, 2022. Revised: August 24, 2023. Accepted: September 29, 2023. Published: October 17, 2023.

## 1 Introduction

The bone remodelling process aims to shape and sculpt the skeleton during growth, to repair micro-damaged bones that occur from everyday stress and also to regulate calcium homeostasis, [1], [2], [3]. It is a significant life-long process, the skeleton is replaced almost 100% in the first year of life while the bone remodelling process of the skeleton occurs approximately 10% per year in adults, [4], [5], [6]. The process involves two types of bone cells, bone tissue will be removed by bone resorbing cells, osteoclasts (OCs), and new bone cells will be formed by bone-forming cells, osteoblasts (OBs), [7]. If the net bone resorption is over the net bone formation after the completion of a bone remodelling cycle, an imbalance will then occur leading to the increase of bone loss and hence, osteoporosis might be expected, [4], [5], [6].

COVID-19 is a contagious disease caused by the SARS-CoV-2. The interaction of SARS-CoV-2

and ACE2 receptors expressed on cellular targets such as alveolar cells of lungs and bone cells enhances the production of inflammatory cytokines, [8]. Also, the binding of SARS-CoV-2 and the ACE2 receptors on osteoclastic cells induces the differentiation of osteoclasts, [8]. However, it has been observed that SARS-CoV-2 also enhances the levels of angiotensin II by downregulating the expression of ACE2 and then induces inflammatory conditions, [9]. Moreover, angiotensin II enhances the differentiation of OCs by enhancing the expression of RANKL on OBs and hence, accelerates the development of osteoporosis in the rat model, [10]. On the other hand, the binding of inflammatory cytokines and cytokine receptors inhibits the osteogenic ability of osteoblasts and hence, bone loss might be increased, [8].

In, [11], the mathematical model developed to investigate the bone remodelling process is as follows.

$$\frac{dP}{dt} = \frac{r_1}{h_1 + C} - s_1 P$$

$$\frac{dC}{dt} = \left( \frac{r_2 + r_3 P}{h_2 + P^2} \right) BC - s_2 C$$

$$\frac{dB}{dt} = r_4 P - \frac{r_5 PB}{h_3 + P} - s_3 B$$

where  $P$  is the PTH concentration above the basal level,  $C$  is the number of active osteoclastic cells and  $B$  is the number of active osteoblastic cells, [1].

Many researchers, [12], [13], [14], [15], [16], [17], [18], [19], also investigated the effects of involving hormones such as estrogen, parathyroid hormone, vitamin D and calcitonin using mathematical modelling. Mathematical models in various forms were developed such as a system of differential equations, a system of delay-differential equations and an impulsive system of differential equations. However, the effects of the inflection with SARS-Cov-2 on the bone remodelling process have never been taken into account. Therefore, the mathematical model developed by, [11], is modified in this paper to investigate bone resorption and bone formation when the effects of the infection with SARS-Cov-2 are also incorporated and the modified model is then analyzed theoretically so that we obtain the conditions for which different dynamics behaviour can be occurred.

## 2 A Modified Mathematical Model and Geometric Singular Perturbation Analysis

In what follows,  $X$  stands for PTH concentration above the basal level at time  $T$ ,  $Y$  stands for the number of active osteoclasts at time  $T$  and  $Z$  stands for the number of active osteoblasts at time  $T$ . The system of differential equations developed by, [11], is modified here to investigate the effects of SARS-Cov-2 on bone resorption and bone formation as follows.

$$\frac{dX}{dT} = \frac{a_1}{k_1 + Y} - b_1 X \quad (1)$$

$$\frac{dY}{dT} = \left( \frac{a_2 + a_3 X}{k_2 + X^2} + \frac{a_4 Y}{k_3 + Y} \right) YZ - b_2 Y \quad (2)$$

$$\frac{dZ}{dT} = a_5 X - \frac{a_6 XZ}{k_4 + X} - a_7 Z - b_3 Z \quad (3)$$

Here, all parametric values in the system of equations (1)-(3) are assumed to be positive.

As described in, [11], the change in PTH concentration in blood above the basal level is represented by equation (1). PTH is assumed to be secreted from the parathyroid gland with the rate presented by the first term on the right-hand side of equation (1) which decreases when the number of active osteoclasts increases so that the calcium levels in blood is maintained to be within the normal range, [11]. PTH is assumed to be removed from the system as represented by the last term of equation (1), [11].

In equation (2), as described in [11], It has been observed that the reproduction of osteoclasts is stimulated by PTH, [20], [21], [22]. However, it has also been observed in, [19], as well that osteoclastic reproduction is inhibited if the level of PTH increases further, the saturation expression  $\frac{a_2 + a_3 X}{k_2 + X^2}$  is then assumed for the stimulating effect of PTH on the osteoclastic reproduction as presented in the first term of the right-hand side of equation (2), [11].

When infected with COVID-19, SARS-Cov-2 will bind with ACE2 receptors on osteoclastic cells and induce the differentiation of osteoclasts, [8]. Moreover, the number of ACE2 receptors available for binding with ACE2 is then decreased resulting in the decrease of the inhibiting effect of ACE2 on osteoclastic reproduction, [23], [24]. Therefore, the number of osteoclastic cells will be increased. Moreover, SARS-CoV-2 also enhances the levels of angiotensin II by downregulating the expression of ACE2, [9]. Angiotensin II then enhances the differentiation of OCs by enhancing the RANKL expression on OBs, [10]. Therefore, the term  $\frac{a_4 Y}{k_3 + Y}$

is assumed on the first term of the right-hand side of equation (2) to account for the effect of COVID-19 on the reproduction of osteoclastic cells. Noted that the effects of both PTH and the infection with COVID-19 on osteoclastic reproduction require the osteoclast differentiation factor (ODF) and its receptor on osteoclastic cells, [19], the term  $YZ$  is then also presented. Active osteoclastic cells are assumed to be removed from the system as presented by the last term on the right-hand side of equation (2), [11].

In equation (3), as described in [11], PTH has been observed to stimulate osteoblastic reproduction and the first term on the right-hand side is then assumed to account for PTH stimulating effect on osteoblastic reproduction, [11]. Moreover, PTH has

also been observed to inhibit osteoblastic reproduction and the second term on the right-hand side is then assumed to account for PTH inhibiting effect on osteoblastic reproduction, [11]. On the other hand, the interaction of SARS-CoV-2 and ACE2 receptors enhances the production of inflammatory cytokines, [8]. Since the binding of inflammatory cytokines and cytokine receptors inhibits the osteogenic ability of osteoblasts, [8], the number of osteoblastic cells will then decrease when infected with COVID-19 and hence the third term on the right-hand side is presented to account for the effect of Covid-19 on the reproduction of osteoblastic cells. Active osteoblastic cells are assumed to be removed from the system by the last term on the right-hand side, [11].

The changes in the levels of PTH in the blood occur within minutes to control the calcium levels in the blood while the bone resorption process takes approximately 2 weeks and the bone formation process takes approximately 3 months, [25], [26]. Hence, we assume that the dynamics of PTH, OCs and OBs are fastest, intermediate and slowest, respectively. We then analyze our modified model by utilizing the geometric singular perturbation technique. Firstly, we scale the variables of the system by two small dimensionless positive parameters  $\varepsilon$  and  $\delta$ . The new parameters are introduced as follows.

Letting

$$x = \frac{X}{X^*}, y = \frac{Y}{Y^*}, z = \frac{Z}{Z^*}, t = \frac{T}{T^*}, c_1 = \frac{T^* a_1}{X^* Y^*}, c_2 = \frac{T^* Z^* a_2}{\varepsilon (X^*)^2},$$

$$c_3 = \frac{T^* Z^* a_3}{\varepsilon X^*}, c_4 = \frac{T^* Z^* a_4}{\varepsilon}, c_5 = \frac{T^* X^* a_5}{\varepsilon \delta Z^*}, c_6 = \frac{T^* a_6}{\varepsilon \delta},$$

$$c_7 = \frac{T^* a_7}{\varepsilon \delta}, m_1 = \frac{k_1}{Y^*}, m_2 = \frac{k_2}{(X^*)^2}, m_3 = \frac{k_3}{Y^*}, d_1 = T^* b_1,$$

$$d_2 = \frac{T^* b_2}{\varepsilon}, \text{ and } d_3 = \frac{T^* b_3}{\varepsilon \delta}, \text{ our model then becomes}$$

$$\frac{dx}{dt} = \frac{c_1}{m_1 + y} - d_1 x \equiv f(x, y, z) \quad (4)$$

$$\frac{dy}{dt} = \varepsilon \left[ \left( \frac{c_2 + c_3 x}{m_2 + x^2} + \frac{c_4 y}{m_3 + y} \right) y z - d_2 y \right] \quad (5)$$

$$\equiv \varepsilon g(x, y, z)$$

$$\frac{dz}{dt} = \varepsilon \delta \left[ c_5 x - \frac{c_6 x z}{m_4 + x} - c_7 z - d_3 z \right] \equiv \varepsilon \delta h(x, y, z) \quad (6)$$

This means that, PTH possesses a faster time response than osteoclasts, while, osteoblasts have slowest dynamics provided that  $\varepsilon$  and  $\delta$  are small

which is consistent with the clinical evidence, [19], [25], [26].

For our system of equations (4)-(6), we now show that the manifolds  $\{f = 0\}$ ,  $\{g = 0\}$  and  $\{h = 0\}$  are shaped and located as shown in Figure 1 (Appendix) and Figure 2 (Appendix) with some appropriate parametric values.

**Manifold  $\{f = 0\}$**

By setting  $\frac{dx}{dt} = 0$  in equation (4), we obtain the manifold  $\{f = 0\}$  which is represented by

$$\frac{c_1}{m_1 + y} - d_1 x = 0$$

or 
$$x = \frac{c_1}{d_1 (m_1 + y)} \equiv r(y)$$

Here,  $r(y)$  is independent of  $z$ . As a result,  $r(y)$  is also parallel to the  $z$ -axis. Moreover, the intersection of  $r(y)$  and the  $(x, z)$ -plane occurs along the straight line

$$x = \frac{c_1}{d_1 m_1} \equiv x_1.$$

In addition, we can see that  $r(y)$  is a decreasing function and

$$\lim_{y \rightarrow \infty} r(y) = \lim_{y \rightarrow \infty} \frac{c_1}{d_1 (m_1 + y)} = 0$$

that is,  $x \rightarrow 0$  as  $y \rightarrow \infty$  along the surface  $x = r(y)$ .

**Manifold  $\{g = 0\}$**

By setting  $\frac{dy}{dt} = 0$  in equation (5), we obtain the manifold  $\{g = 0\}$  which is represented by

$$\left( \frac{c_2 + c_3 x}{m_2 + x^2} + \frac{c_4 y}{m_3 + y} \right) y z - d_2 y = 0$$

or 
$$y \left[ \left( \frac{c_2 + c_3 x}{m_2 + x^2} + \frac{c_4 y}{m_3 + y} \right) z - d_2 \right] = 0$$

composing of two parts, the trivial manifold  $y = 0$ , and the nontrivial manifold

$$z = \frac{(m_2 + x^2)(m_3 + y)}{(c_2 + c_3 x)(m_3 + y) + c_4 y(m_2 + x^2)} \equiv s(x, y)$$

We can see that on the  $(x, z)$ -plane,

$$z = \frac{m_2 + x^2}{c_2 + c_3x} \equiv u(x).$$

Note that  $u(x)$  intersects the  $z$ -axis at the point in which  $x=0$  and  $z = \frac{m_2}{c_2} \equiv z_1$ . Since,

$$u'(x) = \frac{c_3x^2 + 2c_2x - c_3m_2}{(c_2 + c_3x)^2}, u'(x) = 0 \quad \text{is then}$$

occurred in the first octant at the point in which

$$x = -\frac{c_2}{c_3} + \sqrt{\left(\frac{c_2}{c_3}\right)^2 + m_2} \equiv x_2.$$

We remark that  $x_2$  is always positive, when all parameters are assumed to be positive. Moreover,

$$u''(x) = \frac{(2c_3x + 2c_2)}{(c_2 + c_3x)^2} - \frac{2c_3(c_3x^2 + 2c_2x - c_3m_2)}{(c_2 + c_3x)^3}$$

and  $x_2 > 0$ , then

$$u''(x_2) = \frac{(c_2 + c_3x_2)^2(2c_3x_2 + 2c_2)}{(c_2 + c_3x_2)^4} > 0.$$

Therefore,  $z = u(x)$  attains its relative minimum at the point at which  $x = x_2$ ,

$$z = u(x_2) = \frac{m_2 + x_2^2}{c_2 + c_3x_2} \equiv z_2.$$

On the  $(y, z)$ -plane,

$$z = \frac{m_2m_3 + m_2y}{c_2m_3 + (c_2 + c_4m_2)y} \equiv v(y).$$

We can see that,  $v(y)$  intersects the  $y$ -axis at the point for which  $z=0$  and  $y = -m_3$ . Note that

$$\lim_{y \rightarrow \infty} v(y) = \frac{m_2}{c_2 + c_4m_2} \equiv z_*. \quad \text{The intersection of } v(y)$$

and the  $z$ -axis occurs at the point for which  $y = 0$

$$\text{and } z = \frac{m_2}{c_2} = z_1.$$

$$\text{Since } v'(y) = -\frac{c_4m_2^2m_3}{(c_2m_3 + (c_2 + c_4m_2)y)^2} < 0$$

then  $z = v(y)$  is an decreasing function when all parameters are assumed to be positive.

On the  $(x, y)$ -plane,

$$y = -m_3.$$

$$z = \frac{(m_2 + x^2)(m_3 + y)}{(c_2 + c_3x)(m_3 + y) + c_4y(m_2 + x^2)} \equiv s(x, y)$$

Since and

$$\frac{\partial S}{\partial x} = \frac{(m_3 + y)^2(c_3x^2 + 2c_2x - c_3m_2)}{\left[(c_2 + c_3x)(m_3 + y) + c_4y(m_2 + x^2)\right]^2}$$

then  $\frac{\partial S}{\partial x} = 0$  at  $x = x_2$ .

Note that

$$\frac{\partial S}{\partial y} = -\frac{c_4m_3(m_2 + x^2)^2}{\left[(c_2 + c_3x)(m_3 + y) + c_4y(m_2 + x^2)\right]^2} < 0$$

when all parameters are assumed to be positive.

**Manifold**  $\{h=0\}$

By setting  $\frac{dz}{dt} = 0$  in equation (6), we obtain the

manifold  $\{h=0\}$  which is represented by

$$c_5x - \frac{c_6xz}{m_4 + x} - c_7z - d_3z = 0$$

or

$$z = \frac{c_5x(m_4 + x)}{c_6x + (c_7 + d_3)(m_4 + x)} \equiv w(x).$$

Here,  $w(x)$  is parallel to the  $y$ -axis because  $w(x)$  is independent of the variable  $y$ . Also,  $w(x)$  intersects the  $(y, z)$ -plane along the  $y$ -axis.

Since,

$$w'(x) = \frac{c_5(c_6 + c_7 + d_3)x^2}{\left[(c_6 + c_7 + d_3)x + m_4(c_7 + d_3)\right]^2} + \frac{2c_5m_4(c_7 + d_3)x + c_5m_4^2(c_7 + d_3)}{\left[(c_6 + c_7 + d_3)x + m_4(c_7 + d_3)\right]^2}$$

then  $w'(x) = 0$  if

$$(c_6 + c_7 + d_3)x^2 + 2m_4(c_7 + d_3)x + m_4^2(c_7 + d_3) = 0.$$

That is

$$x = -\frac{m_4(c_7 + d_3)}{(c_6 + c_7 + d_3)} \pm \frac{\sqrt{m_4^2(c_7 + d_3)^2 - m_4^2(c_7 + d_3)(c_6 + c_7 + d_3)}}{(c_6 + c_7 + d_3)}$$

< 0

Thus,  $w(x)$  has no relative minimum or maximum where all parametric values are assumed to be positive. Moreover,  $w'(x) > 0$  for  $x > 0$ . Thus,  $w(x)$  is an increasing function in the first octant.

**Theorem 1** Given that  $\varepsilon$  and  $\delta$  are sufficiently small. A limit cycle exists for the system of equations (4)-(6) if the inequalities

$$x_2 < x_3 < x_1, \quad (7)$$

$$y_3 < y_4, \quad (8)$$

and 
$$z_2 < z_3 < z_4 < z_1 \quad (9)$$

hold.

Note that Theorem 1 can be proven by utilizing the geometric singular perturbation techniques, [27], [28].

In Figure 1 (Appendix), the curve  $\{g = h = 0\}$  intersects the curve  $\{f = g = 0\}$  at the point  $S_1$  on the  $(x, z)$ -plane and the point  $S_2$  is located between the points  $(x_2, y_2, z_2)$  and  $(x_1, 0, z_1)$  along the curve  $\{f = g = 0\}$ . Note that the high, intermediate and slow speed transitions are represented by the three, two and one arrows, respectively.

Starting from the generic point  $A = (x_0, y_0, z_0)$  for which  $f(x_0, y_0, z_0) \neq 0$  in Figure 1 (Appendix). Here, the position of point A is assumed to be as shown in Figure 1 (Appendix). A transition in the direction of decreasing  $x$  at a fast speed will bring the solution trajectory from point A to point B located on the manifold  $\{f = 0\}$ , since  $f < 0$  here. Since  $g < 0$  here, a transition of the solution trajectory with an intermediate speed in the direction of decreasing  $y$  will bring the system to the curve  $\{f = g = 0\}$  where a point C is reached. A transition of the solution trajectory in the direction of increasing  $z$  along this curve with a slow speed, since  $h > 0$  here, will then reach some point D on this curve. The stability of the submanifold will be lost and an intermediate transition of the solution trajectory will then bring the system to the other stable part of  $\{f = g = 0\}$  where a point E is reached. A transition of the solution trajectory at slow speed in the direction of decreasing  $z$ , since  $h < 0$  here, will bring the system to the point F in which the stability of the submanifold is lost again. An intermediate transition will then bring the solution trajectory to the other stable part of  $\{f = g = 0\}$  where point G is reached. A transition in the direction of increasing  $z$  with a slow speed will then bring the solution trajectory to point D again, since  $h > 0$  here, resulting in the closed orbit  $DEFG$  and hence, we obtain a limit cycle for our model of equations (4)-(6).

**Theorem 2** Given that  $\varepsilon$  and  $\delta$  are sufficiently small, if the inequalities

$$x_3 < x_2 < x_1, \quad (10)$$

$$y_4 < y_3, \quad (11)$$

and 
$$z_5 < z_3 < z_2 < z_4 < z_1 \quad (12)$$

hold then the equilibrium point  $S_2$  of the system of equations (4)-(6) is stable.

Starting from the generic point  $A = (x_0, y_0, z_0)$  for which  $f(x_0, y_0, z_0) \neq 0$  in Figure 2 (Appendix). The position of A is assumed to be located as in Figure 2 (Appendix). Since  $f < 0$  here, a transition of the solution trajectory in the direction of decreasing  $x$  will bring the system to the manifold  $\{f = 0\}$  with a fast speed where a point B is reached. An intermediate transition of the solution trajectory in the direction of decreasing  $y$  on the curve  $\{f = g = 0\}$  will bring the system to a point C, since  $g < 0$  here. A transition of the solution trajectory along this curve at slow speed in the direction of increasing  $z$ , since  $h > 0$  here, will then bring the system to some point D. The stability of the submanifold will be lost and an intermediate transition of the solution trajectory will then bring the system to the other stable part of  $\{f = g = 0\}$  where a point E is reached. A transition of the solution trajectory at a slow speed in the direction of decreasing  $z$  will bring the system to the equilibrium point  $S_2$  where  $f = g = h = 0$ . Thus, the equilibrium point  $S_2$  is stable.

### 3 Numerical Investigations

In this section, we demonstrate the theoretical predictions by carrying out numerical investigations for each case. All computer simulations are generated by MATLAB using the Runge-Kutta 4th-order method.

In Figure 3 (Appendix), numerical simulation is presented to demonstrate the theoretical result stated in Theorem 1 for which a limit cycle is expected. The parametric values in the system of equations (4)-(6) are chosen to satisfy all inequalities stated in Theorem 1 as follows:  $c_1 = 0.05, c_2 = 0.009, c_3 = 0.675, c_4 = 0.1, c_5 = 0.01, c_6 = 0.005, c_7 = 0.001, m_1 = 0.1, m_2 = 0.5, m_3 = 1, m_4 = 0.025, d_1 = 0.1, d_2 = 0.3, d_3 = 0.01, \varepsilon = 0.1, \delta = 0.9, x(0) = 0.5, y(0) = 0.1,$  and  $z(0) = 0.1$ . In Figure 3 (Appendix), we can see that

a limit cycle exists for the system of equations (4)-(6) and a periodic solution occurs as theoretically predicted in Theorem 1.

In Figure 4 (Appendix), a numerical simulation is presented to demonstrate the theoretical result indicated in Theorem 2. The parametric values in the system of equations (4)-(6) are chosen to satisfy all inequalities stated in Theorem 2 as follows:  $c_1 = 0.05, c_2 = 0.0009, c_3 = 0.882, c_4 = 0.1, c_5 = 0.01, c_6 = 0.005, c_7 = 0.0001, m_1 = 0.1, m_2 = 0.5, m_3 = 1, m_4 = 0.025, d_1 = 0.1, d_2 = 0.3, d_3 = 0.01, \varepsilon = 0.01, \delta = 0.5, x(0) = 0.1, y(0) = 0.5, \text{ and } z(0) = 0.5$ . We can see that the equilibrium point  $S_2$  is stable as theoretically predicted in Theorem 2.

## 4 Discussion

In addition to the numerical simulations represented in Figure 3 (Appendix) and Figure 4 (Appendix), let us consider an example of the computer simulations in Figure 5 (Appendix) for which the number of osteoclasts when there are no effects from SARS-Cov-2 infection ( $c_4 = c_7 = 0$ ) is compared to the number of osteoclasts when there is the effects from SARS-Cov-2 infection ( $c_4 = 0.1, c_7 = 0.001$ ) when the other parameters are the same as the values used in Figure 3 (Appendix). Also, let us consider an example of the computer simulations in Figure 6 (Appendix) for which the number of osteoclasts when there is no effects from SARS-Cov-2 infection ( $c_4 = c_7 = 0$ ) is comparing to the number of osteoclasts when there is the effects from SARS-Cov-2 infection ( $c_4 = 0.1, c_7 = 0.0001$ ) when the other parameters are the same as the values used in Figure 4 (Appendix). We can see that the number of osteoclasts in the cases when there is the effect of SARS-Cov-2 infection is higher than that of the cases when there is no effect of SARS-Cov-2 infection in both Figure 5 (Appendix) and Figure 6 (Appendix) whereas the number of osteoblasts in the cases when there is the effect of SARS-Cov-2 infection is lower than that of the cases when there is no effect of SARS-Cov-2 infection in Figure 6 (Appendix). Therefore, more bone loss might be expected when infected with Covid-19.

## 5 Conclusion

The model developed by, [1], is modified to incorporate the effects of Covid-19 on the reproductions of osteoblastic cells and osteoclastic

cells. The modified model is then analyzed theoretically using the geometric singular perturbation technique so that we obtain the conditions for which different behaviours of solution can be expected. Numerical simulations are also provided to demonstrate the theoretical results. The results indicate that a periodic behaviour which has been observed clinically in the oscillations of the number of osteoclasts and osteoblasts, [19], as well as the pulsatile secretions of PTH, [29], could also be exhibited by our model. In addition, the simulation results in Figure 5 (Appendix) and Figure 6 (Appendix) indicate that the number of osteoclasts in the cases where there is the effect of SARS-Cov-2 infection is higher than that of the cases when there is no effect of SARS-Cov-2 infection whereas the number of osteoblasts in the cases when there is the effect of SARS-Cov-2 infection are lower than that of the cases when there is no effect of SARS-Cov-2 infection and hence, more bone loss can be expected when infected with Covid-19. The modified model in this paper might be modified further to investigate treatments for osteoporosis patients when infected with COVID-19.

### Acknowledgement:

This research has received funding support from the NSRF via the Program Management Unit for Human Resource and institutional Development, Research and Innovation (grant number B05F640231). Also, this research is partially supported by Mahidol University, Thailand.

### References:

- [1] Russell, T., Turner, B., Lawrence, R., Thomas, C.S. Skeletal effects of estrogen. *Endocr. Rev.*, 15(3) (1994): p.275-300.
- [2] Lobo, R.A., Kelsey, J.L. and Marcus, R. *Menopause: Biology and Pathobiology*. Academic Press, 2000, pp. 287-307.
- [3] Albright, J.A. and Sunders, M. *The Scientific Basis of Orthopaedics*. Norwalk, Conn.: Appleton & Lange, 1990.
- [4] Lewellen, T.K., Neip, W.B., Murano, R., Hinn, G.M. and Chesnut, C.H. Absolute Measurement of Total-Body Calcium by the Ar-37 Method- Preliminary Results: Concise Communication. *J. Nucl. Med.*, 18 (1977): p.929-932.
- [5] Morley, P., Whitfield, J.F. and Willick, G.E. Parathyroid hormone: an anabolic treatment

- for osteoporosis. *Curr Phar Design*, 7 (2001): p.671-687.
- [6] Parfitt, A.M. Targeted and nontargeted bone remodelling: relationship to basic multicellular unit origination and progression. *Bone*, 30 (2002): p.5-7.
- [7] Heersche, J.N.M. and Cherk, S. *Metabolic Bone Disease: Cellular and tissue mechanisms*. Boca Raton, FI: CRC Press, 1989.
- [8] Sapra, L., Saini, C., Garg, B., Gupta, R., Verma, B., Mishra, P.K., Srivastava, R.K. Long-term implications of COVID-19 on bone health: pathophysiology and therapeutics. *Inflammation Research*, 71(2022): p.1025-1040.
- [9] Kuba, K., Imai, Y., Penninger, J. Angiotensin-converting enzyme 2 in lung diseases. *Curr Opin Pharmacol*. 6 (2006): 271–6.
- [10] Shimizu, H., Nakagami, H., Osako, M.K., Hanayama, R., Kunugiza, Y., Kizawa, T., Tomita, T., Yoshikawa, H., Ogihara, T., Morishita, R. Angiotensin II accelerates osteoporosis by activating osteoclasts. *FASEB J*. 22(7) (2008): 2465-75.
- [11] Rattanakul, C., Lenbury, Y., Krishnamara, N. and Wollkind, D.J. Mathematical Modelling of Bone Formation and Resorption Mediated by Parathyroid Hormone: Responses to Estrogen/PTH Therapy. *BioSystems*, 70(2003): p.55-72.
- [12] Chaiya I., Rattanakul C., Rattanamongkonkul S., Kunpasurang W., Ruktamatakul S. Effects of Parathyroid Hormone and Calcitonin on Bone Formation and Resorption: Mathematical Modeling Approach. *Int. J. Math. Comp. Simul*. 5(6) (2011): p.510-519.
- [13] Ayati, B.P., Edwards, C.M., Webb, G.F. *et al*. A mathematical model of bone remodeling dynamics for normal bone cell populations and myeloma bone disease. *Biol Direct*. 5(28) (2010).
- [14] Rattanakul C., Rattanamongkonkul S. Effect of Calcitonin on Bone Formation and Resorption: Mathematical Modeling Approach. *Int. J. Mathl. Mod. Meth. Appl. Sci*. 5(8) (2011): p.1363-1371.
- [15] Chen-Charpentiera B.M., Diakite I. A mathematical model of bone remodeling with delays. *Journal of Computational and Applied Mathematics* 291(2016):76–84.
- [16] Chaiya, I., Rattanakul, C. Effects of Prolactin on Bone Remodeling Process with Parathyroid Hormone Supplement: An Impulsive Mathematical Model. *Advances in Difference Equations* (2017) 2017: 147.
- [17] Trejo I., Kojouharov H. A Mathematical Model to Study the Fundamental Functions of Phagocytes and Inflammatory Cytokines During the Bone Fracture Healing Process. *Letters in Biomathematics* 7(1) (2020), p.171–189.
- [18] Aekthong, S., Rattanakul, C. Dynamical Modelling of Bone Formation and Resorption under Impulsive Estrogen Supplement: Effects of Parathyroid Hormone and Prolactin. *International Journal of Mathematics and Mathematical Sciences*. Article ID 5435876, (2021) 17 pages. <https://doi.org/10.1155/2021/5435876>.
- [19] Kroll, M.H. Parathyroid hormone temporal effects on bone formation and resorption. *Bull. Math. Bio*, 62 (2000): p.163-188.
- [20] Dempster, D.W., Cosman, F., Parisisen, M., Shen, V. and Lindsay, R. Anabolic actions of parathyroid hormone on bone. *Endocr Rev*. 14 (1993): p.690-709.
- [21] Weryha, G. and Leclere, J. Paracrine regulation of bone remodeling. *Horm Res*. 43 (1995): p.69-75.
- [22] Brown, E.M. Extracellular Ca<sup>2+</sup> sensing, regulation of parathyroid cell function, and role of Ca<sup>2+</sup> and other ions as extracellular (first) messengers. *Physiol Rev*. 71 (1991): p.371-411.
- [23] Zheng, K., Zhang, W., Xu, Y., Geng, D. Covid-19 and the bone: underestimated to consider. *European Review for Medical and Pharmacological Sciences*. 24 (2020): p.10316-10318.
- [24] Tao, H., Bai, J., Zhang, W., Zheng, K., Guan, P. Ge, G., Li, M., Geng, D. Bone biology and COVID-19 infection: Is ACE2 a potential influence factor? *Medical Hypotheses*. 144 (2020): 110178.
- [25] Whitfield, J.F., Morley, P. and Willick, G.E. *The parathyroid hormone: an unexpected bone builder for treating osteoporosis*. Austin, Tex: Landes Bioscience Company, 1998.
- [26] The epidemiology and pathogenesis of osteoporosis [Online 2002]. Available from <http://www.endotext.org/parathyroid/parathyroid11/parathyroid11.htm>.
- [27] Kaper, T.J. An introduction to geometric methods and dynamical systems theory for singular perturbation problems. Analyzing multiscale phenomena using singular perturbation methods, *Proc. Symposia Appl Math*, 56 (1999).

- [28] Rinaldi, S. and Muratori, S. A separation condition for the existence of limit cycle in slow-fast systems. *Appl Math Modelling*. 15 (1991): p.312-318.
- [29] Prank, K., Harms, H., Brabant, G. and Hesch, R.D. Nonlinear dynamics in pulsatile secretion of parathyroid hormone in normal human subjects. *Chaos*. 5 (1995): p.76-81.

## Appendix

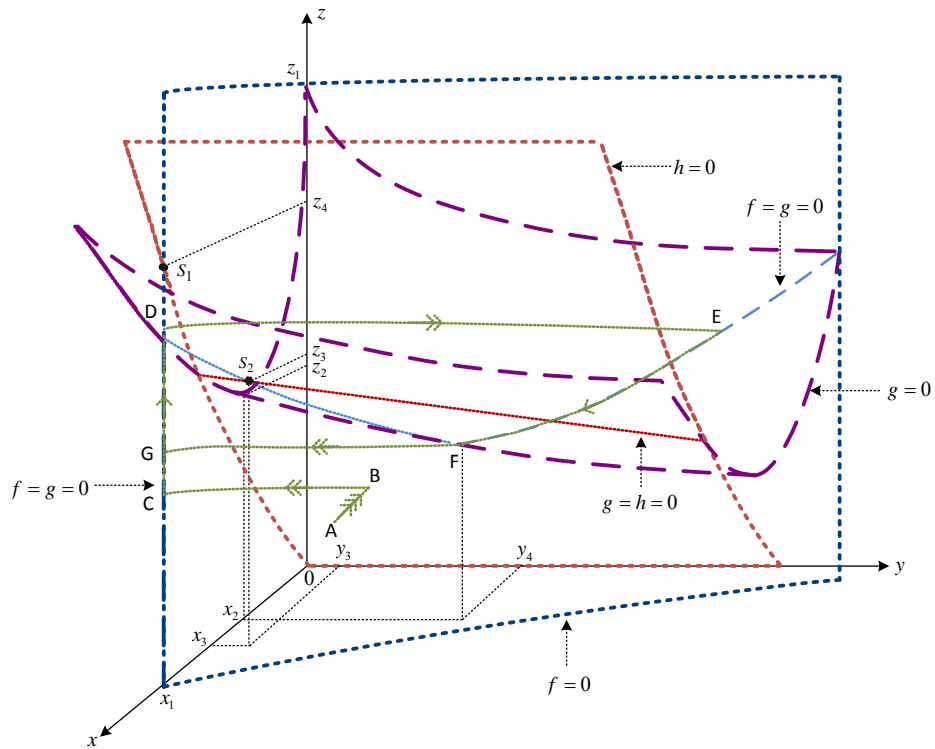


Fig. 1: The manifolds  $\{f=0\}$ ,  $\{g=0\}$  and  $\{h=0\}$  where all conditions in Theorem 1 are satisfied. Here, the fast, intermediate, and slow transitions of the trajectories are represented by three arrows, two arrows, and one arrow, respectively. The solution trajectory tends towards a limit cycle in this case.



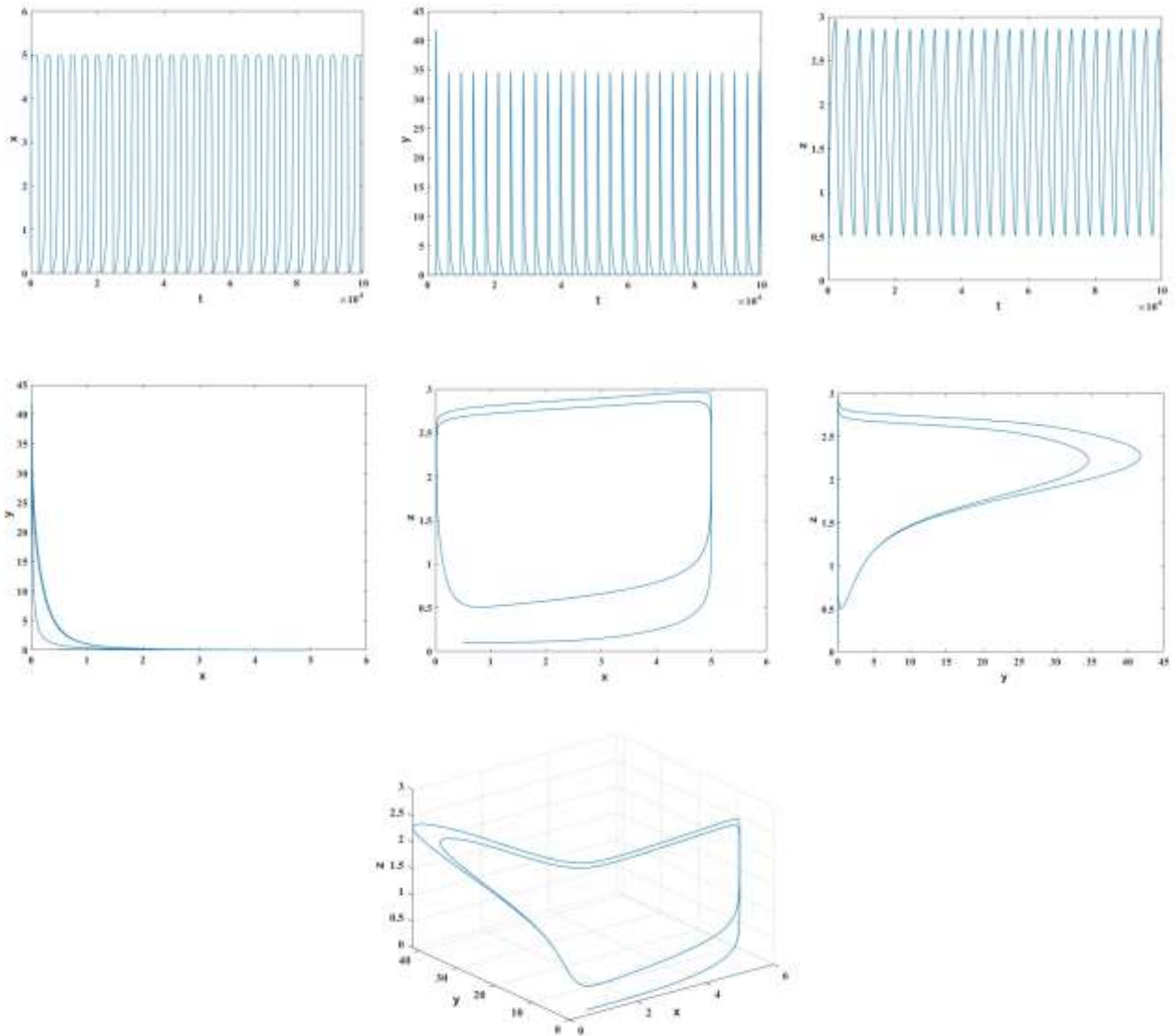


Fig. 3: A numerical simulation of the model system (4)-(6), with the parametric values satisfying all inequalities identified in Theorem 1. Here,  $c_1 = 0.05, c_2 = 0.009, c_3 = 0.675, c_4 = 0.1, c_5 = 0.01, c_6 = 0.005, c_7 = 0.001, m_1 = 0.1, m_2 = 0.5, m_3 = 1, m_4 = 0.025, d_1 = 0.1, d_2 = 0.3, d_3 = 0.01, \varepsilon = 0.1, \delta = 0.9, x(0) = 0.5, y(0) = 0.1,$  and  $z(0) = 0.1$ . A limit cycle exists as predicted in Theorem 1.

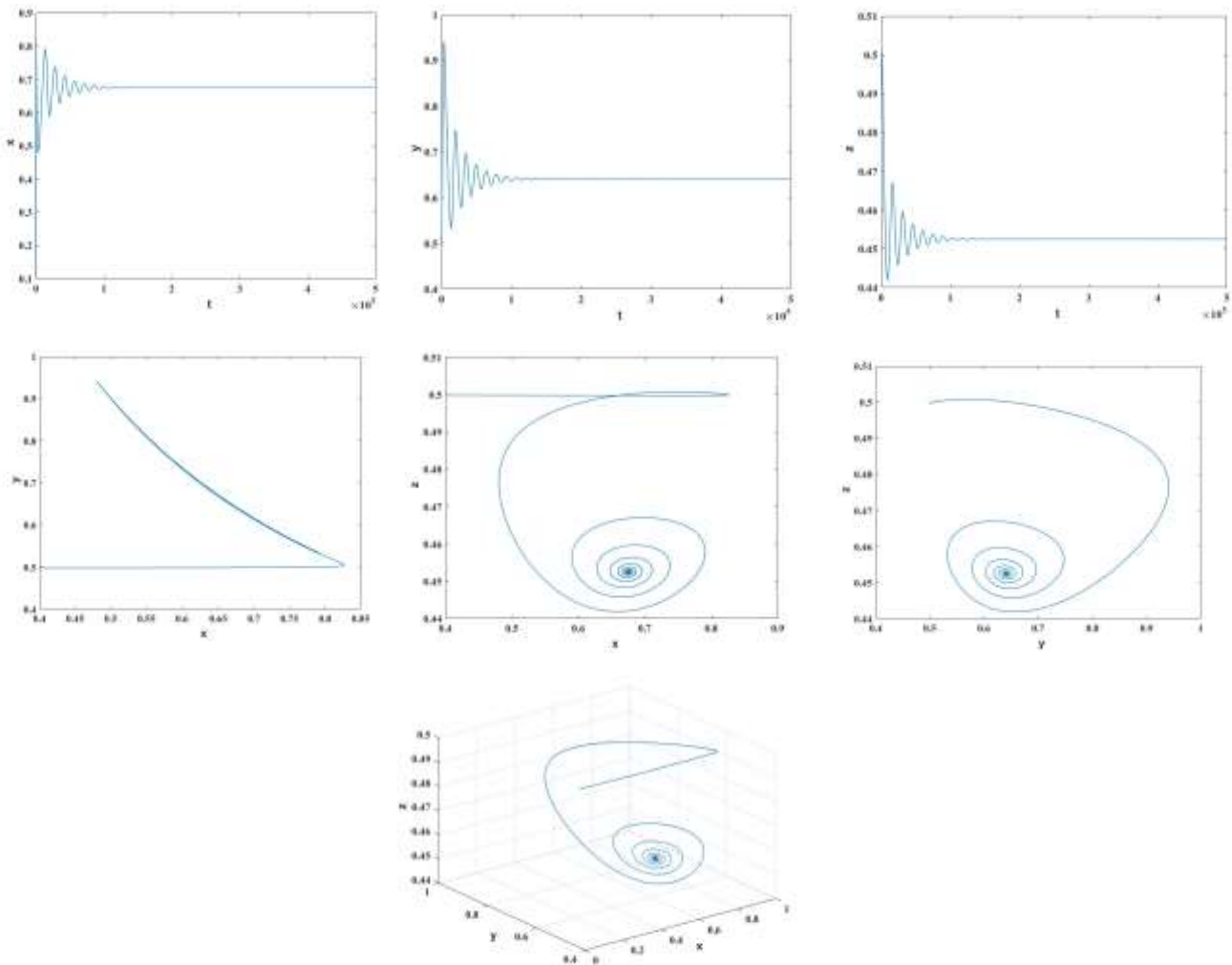


Fig. 4: A numerical simulation of the model system (4)-(6), with parametric values satisfying all inequalities stated in Theorem 2. Here,  $c_1 = 0.05, c_2 = 0.0009, c_3 = 0.882, c_4 = 0.1, c_5 = 0.01, c_6 = 0.005, c_7 = 0.0001, m_1 = 0.1, m_2 = 0.5, m_3 = 1, m_4 = 0.025, d_1 = 0.1, d_2 = 0.3, d_3 = 0.01, \varepsilon = 0.01, \delta = 0.5, x(0) = 0.1, y(0) = 0.5,$  and  $z(0) = 0.5$ . The equilibrium point  $S_2$  is stable as predicted in Theorem 2.

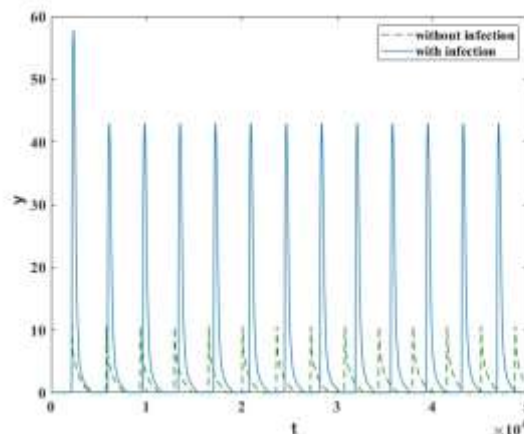


Fig. 5: Comparison of the numerical simulations of the system of equations (4)-(6) for the case when  $c_4 = c_7 = 0$  (without effects of SARS-Cov-2 infection) and  $c_4 = 0.1, c_7 = 0.001$  (with effects of SARS-Cov-2 infection). Here,  $c_1 = 0.05, c_2 = 0.009, c_3 = 0.675, c_5 = 0.01, c_6 = 0.005, m_1 = 0.1, m_2 = 0.5, m_3 = 1, m_4 = 0.025, d_1 = 0.1, d_2 = 0.3, d_3 = 0.01, \varepsilon = 0.1, \delta = 0.9, x(0) = 0.5, y(0) = 0.1, z(0) = 0.1$ .

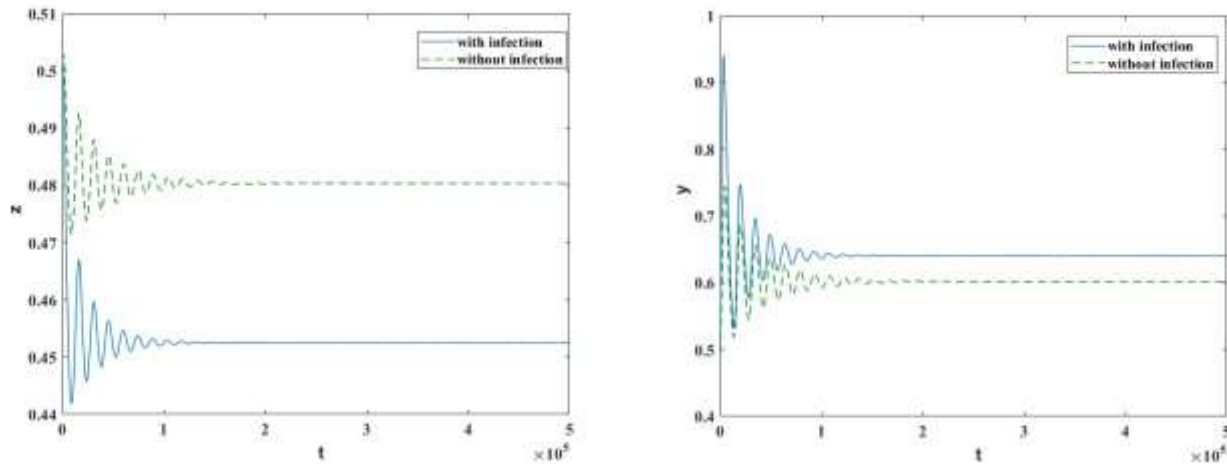


Fig. 6: Comparison of the numerical simulations of the system of equations (4)-(6) for the case when  $c_4 = c_7 = 0$  (without effects of SARS-Cov-2 infection) and  $c_4 = 0.1, c_7 = 0.0001$  (with effects of SARS-Cov-2 infection). Here,  $c_1 = 0.05, c_2 = 0.0009, c_3 = 0.882, c_5 = 0.01, c_6 = 0.005, m_1 = 0.1, m_2 = 0.5, m_3 = 1, m_4 = 0.025, d_1 = 0.1, d_2 = 0.3, d_3 = 0.01, \varepsilon = 0.01, \delta = 0.5, x(0) = 0.1, y(0) = 0.5, z(0) = 0.5$ .

**Contribution of Individual Authors to the Creation of a Scientific Article (Ghostwriting Policy)**

The author contributed in the present research at all stages including the formulation of the problem, the theoretical analysis of the model, numerical investigations as well as preparation of the manuscripts.

**Sources of Funding for Research Presented in a Scientific Article or Scientific Article Itself**

This research has received funding support from the NSRF via the Program Management Unit for Human Resource and institutional Development, Research and Innovation (grant number B05F640231). Also, this research is partially supported by Mahidol University, Thailand.

**Conflict of Interest**

The author has no conflicts of interest to declare that are relevant to the content of this article.

**Creative Commons Attribution License 4.0 (Attribution 4.0 International, CC BY 4.0)**

This article is published under the terms of the Creative Commons Attribution License 4.0 [https://creativecommons.org/licenses/by/4.0/deed.en\\_US](https://creativecommons.org/licenses/by/4.0/deed.en_US)